Design and Optimization of Microring Resonators in Biochemical Sensing Applications

Chung-Yen Chao and L. Jay Guo, *Member, IEEE*

***Abstract*—Microring resonators can be exploited for biochemical sensing applications. To gain a better understanding of the design and optimization of microring sensors, the authors analytically derive the detection limit and the sensitivity. Other important parameters, including the ON–OFF contrast ratio and the signal-to-noise ratio (SNR), are also considered. In this paper, the combination of two sensing mechanisms and two sensing schemes are analyzed. These calculations provide a guideline for determining the microring geometry to satisfy the desired sensing requirements. In addition, the results can provide insights on how to enhance the sensitivity and lower the detection limit.**

***Index Terms*—Biochemical sensors, biosensors, integrated optics, microcavity, microresonator, microring, microring resonator, optical waveguides, ridge waveguides, sensors, waveguide.**

I. Introduction

BIOLOGICAL and chemical sensors have been active research topics because of many potential applications in, to name a few, clinical screening, medical diagnostics, screening of chemical compounds in drug discovery and development, food safety, and environment monitoring. Among the existing biological and chemical sensors, sensors based on integrated optical waveguides have been demonstrated to possess a promising performance. These include planar optical-waveguide sensors [1], directional coupler sensors [2], Mach–Zehnder interferometric sensors [3], grating-coupled waveguide sensors [4], [5], and microresonator sensors [6]–[10]. Integrated optical-waveguide sensors render a number of attractive properties including robustness, compactness for use outside laboratories, high surface specificity using surface chemical modifications, easy patterning of reagents, and high integration capability with electronic and photonic devices. In addition, they are compatible with microfluidic handling and can accommodate multichannel (multianalyte) sensing.

Most optical-waveguide sensors rely on evanescent wave sensing to interrogate the presence of analytes adsorbed on sensor surface or in the surrounding medium. The existence of analytes changes the refractive index close to the sensor surface and, in turn, the effective index of the guided mode, which is probed by an evanescent wave. Such a sensing scheme eliminates the need of fluorescently labeling the analytes and facilitates the label-free detection. In order to detect a low concentration or minute amount of analytes, a long interaction length (i.e., large device size, typically in the range of centimeters for straight-waveguide sensors) is often required to accumulate a detectable phase shift and obtain a reliable signal-to-noise ratio (SNR). It also means that a significant amount of analytes is needed, which might not be available in many applications. This issue can be addressed using microresonator sensors.

Recently, microresonators have been proposed for sensing applications [10]–[12]. These devices offer a unique advantage of reducing the device size by orders of magnitude without sacrificing the interaction length by virtue of their high quality-factor (Q) resonance. The resonance effect provides an equivalently long interaction length to achieve a sufficient phase shift. Such a property can dramatically reduce the device size and the amount of analytes needed for detection. For example, the microsphere resonator, which is one type of microresonator using the whispering-gallery mode (WGM) resonance, has been demonstrated to respond to a monolayer of protein adsorption [8]. Microring resonators have been illustrated to distinguish minute concentration changes of glucose [10]. Microdisk resonators have been predicted to provide sensitivity enhancement and analyte reduction by at least one order of magnitude in comparison with straight-waveguide sensors [11].

Intuitively, a higher Q factor should lead to a better detection limit. The Q of a device depends on the geometry of the microring and the loss in the microcavity (in this paper, we neglect the influence of the material loss in the design consideration). On the other hand, the sensor is based on an evanescent wave interacting with the analytes surrounding the waveguide, the cross-section geometry of which would have a strong effect on the device sensitivity. A smaller cross section would allow a higher evanescent field outside the waveguide and at the same time would increase the waveguide loss. Clearly, a systematic analysis of the device performance is needed in order to evaluate the influence of various device design parameters on the ultimate detection limit.

In this paper, the sensitivity and the detection limit of microring resonators are derived. Based on the calculations, a detailed estimation of the sensor performance is presented for several examples. These illustrations provide some general guidelines in obtaining optimal microring geometries to satisfy the desired sensing requirement.

II. Theory

A. Microring Resonators

A basic microring resonator consists of a ring waveguide as a resonant cavity, which is closely coupled with one (singly

Manuscript received May 17, 2005; revised September 8, 2005. This work was supported in part by the National Institute of Health, the University of Michigan's Technology Transfer Office, and the MUCI challenge fund.

The authors are with the Department of Electrical Engineering and Computer Science, University of Michigan, Ann Arbor, MI 48109 USA (e-mail: guo@umich.edu).

Digital Object Identifier 10.1109/JLT.2005.863333

0733-8724/$20.00 © 2006 IEEE

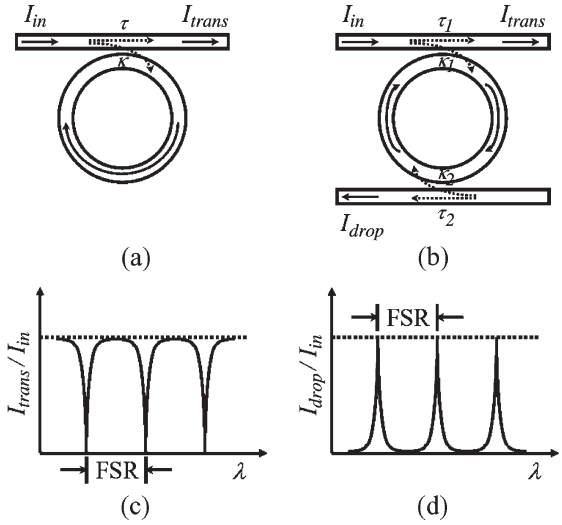

Fig. 1. Basic configurations of microring resonators. (a) Singly coupled microring and (b) a doubly coupled microring. (c) Transmitted ports in both configurations have a spectrum of periodic-notch resonance. (d) Drop port in the doubly coupled configuration has a complementary periodic peak resonance spectrum.

coupled) or two (doubly coupled) straight bus waveguides serving as the input and the output, as shown in Fig. 1(a) and (b), respectively. These waveguide structures can be analyzed to relate the output intensity to the incident intensity [13]. For a singly coupled microring, the transmission coefficient, defined as the ratio of the transmitted intensity to the incident intensity, can be expressed as

$$T \equiv \frac{I_{\rm trans}}{I_{\rm in}} = \left| \frac{\alpha_i \tau - \alpha_i^2 a {\rm e}^{j\phi}}{1 - \alpha_i a \tau {\rm e}^{j\phi}} \right|^2 \tag{1}$$

where α_i is the coupling loss, τ is the amplitude self-coupling coefficient, κ is the amplitude cross-coupling coefficient, a is the amplitude attenuation factor in the ring waveguide, and ϕ is the single-pass phase shift of the wave propagating in the microring. Equation (1) implies that the transmission has a periodic-notch spectrum as plotted in Fig. 1(c). From this equation, the resonance condition is obtained as

$$\lambda_{\rm c} = \frac{n_{\rm eff} L}{m} \tag{2}$$

where $\lambda_{\rm c}$ is the resonant wavelength, $n_{\rm eff}$ is the effective index of the guided mode, L is the circumference of the microring, and m is an integer representing the resonance order.

For a doubly coupled configuration, there are two outputs: the transmission port and the drop port. According to experimental results [14], drop ports have a lower background disturbance and a higher intensity contrast between ON and OFF resonance. These properties facilitate sensing applications. Using the same electromagnetic theory and assuming two identical couplers, the transmission coefficient at the drop port, which is defined as the ratio of the dropped intensity to the incident intensity, can be expressed as

$$T_{\rm d} \equiv \frac{I_{\rm drop}}{I_{\rm in}} = \left| \frac{\alpha_i^2 \sqrt{a} \kappa^2 {\rm e}^{j\phi}}{1 - \alpha_i^2 a \tau^2 {\rm e}^{j\phi}} \right|^2. \tag{3}$$

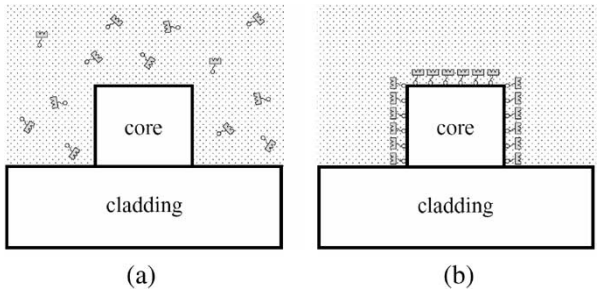

Fig. 2. Two sensing mechanisms. (a) Homogeneous sensing where analytes exist in the surrounding aqueous medium that serves as the top cladding. (b) Surface sensing where analyte molecules adsorb on a sensor surface, which can be modeled as an ultrathin film.

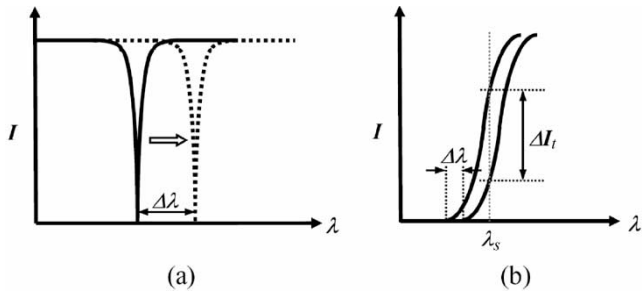

Fig. 3. Two sensing schemes measuring (a) resonant-wavelength shift and (b) intensity variation.

Based on the calculation, a doubly coupled microring has a similar periodic-notch spectrum to the singly coupled case in the transmission port and a complementary peak spectrum in the drop port shown in Fig. 1(d). The resonance condition is still the same as in (2).

B. Sensitivity

For optical-waveguide sensors, there are two sensing mechanisms that are commonly used: homogeneous sensing and surface sensing [14], as shown in Fig. 2. In homogeneous sensing, the device is typically surrounded with an analyte solution, which can be regarded as the top cladding of the waveguide. The homogeneously distributed analyte in the solution will modify the bulk refractive index of the solution. Such an index modification changes the effective index of the guided mode. In this mechanism, all materials including the detected analyte in the solution can contribute to the effective-index shift, which leads to no specificity. To solve this problem, surface sensing can be employed. In surface sensing, the optical device is pretreated to have receptors or binding sites on the sensor surfaces [8], which can selectively bind the specific analyte. Accordingly, this method enables a specificity as well as a label-free detection. In addition, this method can provide a higher sensitivity due to the presence of a larger evanescent field at the waveguide boundary to probe the analytes.

To transduce the amount of analytes to a detectable signal of a microring sensor, two sensing schemes can be used: the resonant-wavelength-shift scheme and the intensity-variation scheme [10], as shown in Fig. 3. The former scheme monitors the shift of a resonant wavelength caused by analytes. It provides a wider detection range but requires a more sophisticated

TABLE I
OVERALL SENSITIVITY S OF A MICRORING SENSOR IS DEFINED BASED ON TWO SENSING MECHANISMS (HOMOGENEOUS AND SURFACE SENSING) AND TWO SENSING SCHEMES (RESONANT-WAVELENGTH-SHIFT SCHEME AND INTENSITY-VARIATION SCHEME). SENSITIVITY IN EACH OF THE FOUR CASES IS EXPRESSED AS A MULTIPLICATION OF THE DEVICE SENSITIVITY AND THE WAVEGUIDE SENSITIVITY. IN THE INTENSITY-VARIATION SCHEME, I REPRESENTS THE MEASURED INTENSITY, WHICH CAN EITHER BE I_{trans} OR I_{drop}

		Sensing Scheme	
		resonant wavelength shift	intensity variation
Sensing Mechanism	homogeneous	$S \equiv \frac{\partial \lambda_c}{\partial n_c} = \frac{\partial \lambda_c}{\partial n_{eff}} \cdot \frac{\partial n_{eff}}{\partial n_c}$	$S \equiv \frac{\partial I}{\partial n_c} = \frac{\partial I}{\partial n_{eff}} \cdot \frac{\partial n_{eff}}{\partial n_c}$
	surface	$S \equiv \frac{\partial \lambda_c}{\partial t} = \frac{\partial \lambda_c}{\partial n_{eff}} \cdot \frac{\partial n_{eff}}{\partial t}$	$S \equiv \frac{\partial I}{\partial t} = \frac{\partial I}{\partial n_{eff}} \cdot \frac{\partial n_{eff}}{\partial t}$

setup owing to the spectrum measurement. The latter scheme monitors the output intensity variation at the wavelength with the highest slope in the transmission spectrum. Such a steep slope is able to convert a tiny shift of a resonant wavelength to a much larger detectable intensity variation. Thus, this scheme can potentially provide a higher sensitivity and a simpler setup without the need of a spectrum measurement. However, it only functions when the monitoring wavelength lies close to the selected resonance, and this leads to a smaller dynamic range.

To evaluate and compare the device performance, we define the sensitivity as the ratio of the change in the measured optical parameter (i.e., λ_{c} in the resonant-wavelength-shift scheme and I_{trans} or I_{drop} in the intensity-variation scheme) to the change in the waveguide parameter affected by analytes (cladding index n_{c} in homogeneous sensing and adsorbed film thickness t in surface sensing). According to the definition, the sensitivity S for four different combinations is listed in Table I. From the mathematical expression, it can be seen that the sensitivity can be further divided into two parts, which we call device sensitivity and waveguide sensitivity, respectively. The device sensitivity is defined as the ratio of the change in the measured optical parameter to the effective-index change, while the waveguide sensitivity is the ratio of the effective-index change to the change in the waveguide parameter affected by analytes. The device sensitivity only depends on the device property, and the waveguide sensitivity is relevant to a waveguide structure regardless of the type of devices. These two parts can be enhanced separately to achieve a higher overall sensitivity.

The device sensitivity is related to the measured optical parameter, which implies that it depends on sensing schemes. For a resonant-wavelength-shift scheme, the device sensitivity can be derived from (2) as

$$(S_{\mathrm{d}})_{\mathrm{RWS}} \equiv \frac{\partial \lambda_{\mathrm{c}}}{\partial n_{\mathrm{eff}}} = \frac{\lambda_{\mathrm{c}}}{n_{\mathrm{eff}}} = \frac{L}{m} \tag{4}$$

while for the intensity-variation scheme, it becomes

$$(S_{\mathrm{d}})_{\mathrm{IV}} \equiv \frac{\partial I}{\partial n_{\mathrm{eff}}} = \frac{\lambda_{\mathrm{c}} \cdot s}{n_{\mathrm{eff}}} = \frac{L \cdot s}{m} \tag{5}$$

where s is the spectrum slope at the detecting wavelength, and I is the measured optical intensity.

The waveguide sensitivity is related to the waveguide parameter affected by analytes. In homogeneous sensing, analytes modify the index of the top cladding; in surface sensing, they change the waveguide cross section due to the adsorbed biomolecular film. This implies that the waveguide sensitivity depends on sensing mechanisms. For homogeneous sensing, the waveguide sensitivity is defined as $\partial n_{\mathrm{eff}}/\partial n_{\mathrm{c}}$. Using the basic waveguide theory and the effective-index method, the waveguide sensitivity can be calculated for both TE and TM polarizations, respectively, as

$$(S_{\mathrm{w}})_{\mathrm{h,TE}} = \frac{n_{\mathrm{cl}}}{n_{\mathrm{eff}}} \times \frac{1 + \frac{2\gamma_{\mathrm{c}} k_x}{n_{\mathrm{co}}^2 k_0^2} \tan\left(\frac{k_x W}{2}\right)}{1 + \frac{n_{\mathrm{cl}}^2 \gamma_{\mathrm{c}}}{n_{\mathrm{co}}^2 k_x}\left[\tan\left(\frac{k_x W}{2}\right) + \frac{k_x W}{2}\sec^2\left(\frac{k_x W}{2}\right)\right]} \tag{6}$$

and

$$(S_{\mathrm{w}})_{\mathrm{h,TM}} = \left\{\frac{n_{\mathrm{eff}}}{n_{\mathrm{cl}}}\left[1 + \frac{\gamma_{\mathrm{c}}}{k_x}\tan\left(\frac{k_x W}{2}\right) + \frac{\gamma_{\mathrm{c}} W}{2}\sec^2\left(\frac{k_x W}{2}\right)\right]\right\}^{-1} \tag{7}$$

where W is the waveguide width. The definition of all other parameters used in the above equations and the details of the derivation can be found in Appendix I.

For surface sensing, the waveguide sensitivity is defined as $\partial n_{\mathrm{eff}}/\partial t$. Again, with use of the same theory, it can be expressed as

$$(S_{\mathrm{w}})_{\mathrm{s,TE}}^{-1} = \frac{n_{\mathrm{eff}}(A-1)^{-2}}{n_{\mathrm{f}}^2 - n_{\mathrm{cl}}^2} \times \left\{-\frac{2A}{k_0^2 n_{\mathrm{eff}}^2} \cdot \left[\gamma_{\mathrm{c}} - \frac{n_{\mathrm{cl}}^2}{n_{\mathrm{co}}^2} k_x B\right] + (A-1) \times \left[\frac{1}{\gamma_{\mathrm{c}}} + \frac{W n_{\mathrm{cl}}^2}{2 n_{\mathrm{co}}^2}(1 + B^2) + \frac{n_{\mathrm{cl}}^2}{n_{\mathrm{co}}^2 k_x} B\right]\right\} \tag{8}$$

and

$$(S_{\mathrm{w}})_{\mathrm{s,TM}}^{-1} = \frac{n_{\mathrm{eff}}}{n_{\mathrm{f}}^2 - n_{\mathrm{cl}}^2} \times \left[\frac{1}{\gamma_{\mathrm{c}}} + \frac{1}{k_x}\tan\left(\frac{k_x W}{2}\right) + \frac{W}{2}\sec^2\left(\frac{k_x W}{2}\right)\right] \tag{9}$$

for TE and TM polarizations, respectively. The definition of all parameters used and the details of the derivation can be found in Appendix II.

C. Detection Limit

In most biological and chemical sensors, the detection limit is a very important parameter to evaluate the sensing capability of a device. The detection limit is typically defined as the smallest detectable change of the waveguide parameters

caused by analytes, which is directly related to the smallest analyte amount that a sensor can detect. The detection limit is proportional to the smallest detectable index change of the top cladding δn_{c} for the case of microring sensors utilizing resonant-wavelength-shift monitoring as the sensing scheme and to the smallest detectable thickness change of the adsorbed analyte film δt for the case in surface sensing. According to the definitions of sensitivity, the detection limit is then proportional to $\delta\lambda_{\mathrm{c}}/S$, where $\delta\lambda_{\mathrm{c}}$ is the distinguishable wavelength shift. Theoretically, $\delta\lambda_{\mathrm{c}}$ is independent of the resonance shape or the resonant bandwidth and should be determined merely by the instrument resolution. However, in reality, a noise can perturb the resonance spectrum such that the accurate detection of resonant-wavelength shift becomes difficult for a broad resonance line shape. To enhance the accuracy in detecting the wavelength shift, a narrower resonance is required. This is equivalent to obtaining a higher Q resonance behavior, where Q is defined as the ratio of a resonant wavelength to its bandwidth.

Experimentally, $\delta\lambda_{\mathrm{c}}$ can be taken as a fraction of the bandwidth of the resonance, which is defined as the full width at half maximum (FWHM) of the resonance. The sharper the resonance, the smaller $\delta\lambda_{\mathrm{c}}$ can be achieved. Hence, the detection limit is proportional to FWHM$/S$ or $1/(Q\cdot S)$, where Q is the quality factor of a resonance. To evaluate the performance of a microring sensor, we define a detection factor $P=\mathrm{FWHM}/S$. In the design of sensors, a smaller detection factor is desired.

Based on our calculation and experiments [14], microring sensors with a Q of 20 000 have a detection limit of $\sim 10^{-5}$ refractive index unit (RIU) using homogeneous sensing and the resonant-wavelength-shift scheme assuming that $\delta\lambda_{\mathrm{c}}$ is 10 pm. The detection limit is smaller by employing surface sensing and/or the intensity-variation scheme. With a proper environment control, such as the temperature, the limit can be further lowered due to a reduction of $\delta\lambda_{\mathrm{c}}$.

III. Design Consideration

In sensing applications using microrings, there are several criteria that need to be fulfilled. For the singly coupled case, a low detection limit and a high sensitivity are required. In addition, a contrast ratio between ON and OFF resonance should be sufficiently large to avoid the noise disturbance, to increase the SNR, and to easily distinguish the resonance. A higher contrast ratio can also greatly enhance the sensitivity when using an intensity-variation scheme due to steeper spectrum slopes. In order to obtain the highest contrast ratio, microring resonators should be operated at the critically coupled point, which means that the energy coupled into the resonator is balanced with the loss energy inside the resonator ($\tau=\alpha_i a$). In this situation, the transmission at resonance is 0 according to (1). Moreover, the nonresonance transmission should remain high enough to have a distinctive resonance behavior. For a doubly coupled microring using its drop port in sensing, most requirements in singly coupled case are still valid: low detection limit, high sensitivity, and high contrast ratio. Moreover, a large on-resonance dropping coefficient is desired to enhance the SNR.

In addition to the aforementioned requirements, a large detection range is pursued, which can be achieved by tracking the resonance [8]. However, if the acquisition time is slower than the reaction time, the detection range is limited by an adjacent resonance. In this situation, it is desirable to have a wider free spectrum range (FSR), which is defined as the difference between two adjacent resonant wavelengths. From (1) and (3), the FSR for each propagation mode can be calculated as

$$\mathrm{FSR}=\frac{\lambda_{\mathrm{c}}^2}{L\cdot\left(n_{\mathrm{eff}}-\lambda_{\mathrm{c}}\frac{\partial n_{\mathrm{eff}}}{\partial\lambda_{\mathrm{c}}}\right)}=\frac{\lambda_{\mathrm{c}}^2}{L\cdot n_{\mathrm{g}}} \tag{10}$$

where n_{g} is the group velocity. From this equation, the FSR is inversely proportional to the ring size. A sufficiently large FSR sets the upper limit of the radius of the microring. Another criterion is to have a single-mode propagation in microring waveguides. Such a design can eliminate the drawbacks in a multimode waveguide where each mode can create its own periodic resonance and the resonances from different modes may be too close to distinguish. A single-mode propagation can also provide a wider FSR for a wider detection range in applications of fast reactions and leads to a simpler spectrum. This criterion sets the upper limit of the waveguide width. According to the last two criteria, a working window in terms of the waveguide width and the radius of the microring can be determined.

IV. Examples

Microring sensors have recently been demonstrated using polymers [10] with advantages including low cost, simple film preparation, and simple fabrication processes [15]. We focus on polymer microring sensors in the following design cases. It should be noted that the design method could also be applied to microring sensors using other materials.

For a microring structure, the most important parameters are the waveguide width W and the radius of microring R_{c}. We search for the optimal W and R_{c} to obtain the best sensing performance. According to (2), different R_{c}s can cause different resonant wavelengths where $L=2\pi R_{\mathrm{c}}$ is used. A different W also corresponds to different resonant wavelengths because n_{eff} is dependent on W. To achieve a systematic and reasonable analysis, we choose the resonance order m such that when W is varied, the corresponding resonant wavelength lies within the same range for each R_{c}. For cases with varied Ws and a specific R_{c}, m is kept unchanged.

In the following cases, we consider a polystyrene microring sensor using resonant-wavelength-shift scheme as an example. The polystyrene microring sits on a 3.66-μm-thick SiO_2 and Si substrate. The microring is a ridge waveguide structure with a polystyrene core of 1.8 μm in thickness. In sensing applications, the detecting devices are typically immersed in aqueous environments. Thus, water is assumed to cover the device and serves as the top cladding. The indices of water, polystyrene, SiO_2, and Si near 1550 nm are 1.3109, 1.57, 1.444, and 3.42, respectively. To simplify the calculation, the coupling loss in the coupling region is neglected, i.e, $\alpha_i=1$. The design

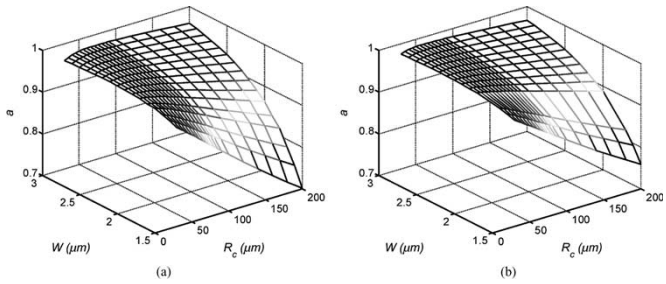

Fig. 4. Amplitude attenuation factor in the ring waveguide as a function of W and R_c plotted for (a) TE and (b) TM fundamental modes.

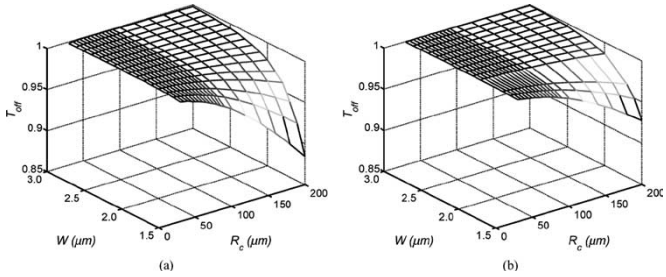

Fig. 5. Nonresonance transmission in the ring waveguide as a function of W and R_c plotted for (a) TE and (b) TM fundamental modes.

requires calculation of τ and a defined as the ratio of the E field after propagating one round trip inside a ring waveguide to that before propagation. The former is obtained using the coupled-mode theory [13], while the latter is calculated from the waveguide loss in the microring [16].

The amplitude attenuation factor in the ring waveguide a, which is a measure of propagation loss in the ring, is related to the waveguide structure and R_c. For both singly coupled and doubly coupled microrings, a is identical and is shown in Fig. 4 for TE and TM polarizations. From Fig. 4, when R_c is too large, a decreases or the loss inside microring resonators increases. It is obvious that a larger device size produces a higher loss when the loss per unit length is nearly constant. This phenomenon is more severe for narrow waveguides due to the higher cavity loss. For typical microring resonators, the main loss comes from surface roughness scattering, which increases with the E field at the core-cladding boundaries. Thus, narrow waveguides have higher cavity losses due to larger E fields at the boundaries.

To satisfy the criteria of single-mode propagation and sufficiently larger FSR, the simulations are performed within a window of W ranging from 1.5 μm to 3 μm and R_c ranging from 30 to 200 μm.

A. Singly Coupled Microring Sensor at Critical Coupling

Singly coupled microrings have the highest contrast ratios when critical coupling $(\tau = \alpha_i a)$ is achieved. Using the critical-coupling condition, the nonresonance transmission T_{off} can be calculated from (1) as functions of the waveguide width W and the radius of the microring R_c for both TE and TM polarizations shown in Fig. 5. These figures illustrate that a narrower W and a larger R_c lead to a smaller nonresonance transmission because of the increase of the loss in the microring. Even though the nonresonance transmission drops, the contrast ratio can still be maintained to exceed 10 for practical applications.

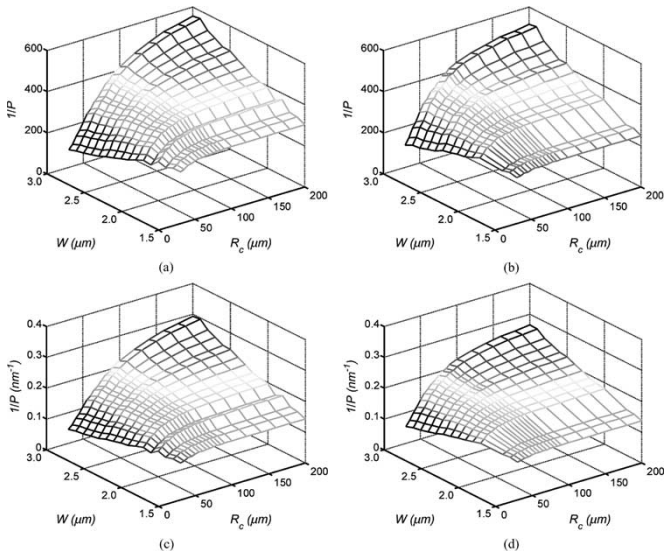

Fig. 6. Inverse of the detection factor plotted as a function of W and R_c for (a) TE and (b) TM fundamental modes in the case of homogeneous sensing and for (c) TE and (d) TM fundamental modes in the case of surface sensing, respectively. All plots show that a minimal P occurs at a larger W and R_c.

In sensing applications, the detection limit, which is proportional to the detection factor P, should be minimized. This relationship is valid for a resonance-shift detection scheme and an intensity-variation detection scheme. The FWHM can be estimated from (1) and the sensitivity can be calculated according to (4) and (6)–(9). For convenience, the inverse of the detection factor $1/P$ is used for three-dimensional (3-D) plotting, which is shown in Fig. 6 for both homogeneous-sensing and surface-sensing schemes. These figures illustrate that the lower detection limit, i.e., smaller P, occurs at a wider waveguide width and a larger radius of microring. This behavior can be understood by separately analyzing Q and the sensitivity dependence on W and R_c.

Using the derived sensitivity equations, the overall sensitivity is obtained as shown in Fig. 7 for the cases of homogeneous and surface sensing. It is shown that the overall sensitivity has little dependence on R_c. The reasons are as follows. First, the waveguide sensitivity is independent of R_c and the device sensitivity from (4) has a weak dependence on R_c. On the contrary, the overall sensitivity decreases with an increase of W. This is because the waveguide-based sensors rely on evanescent waves to interrogate analytes. With narrower waveguides, the evanescent waves can extend more into aqueous top cladding and create a larger impact on modifying n_{eff}. This feature can shift the resonant wavelength more such that the sensitivity is enhanced. On the other hand, we also need to keep in mind that the waveguides cannot be too narrow due to an increase of the propagation loss.

The influence of FWHM can be examined using Q, which is inversely proportional to the FWHM. Q is plotted in Fig. 8 as a function of W and R_c for TE and TM modes. It is shown that a larger Q occurs at a larger W and R_c. This can be understood, because Q represents the ratio of the energy stored in a resonator to the energy loss per cycle. According to this

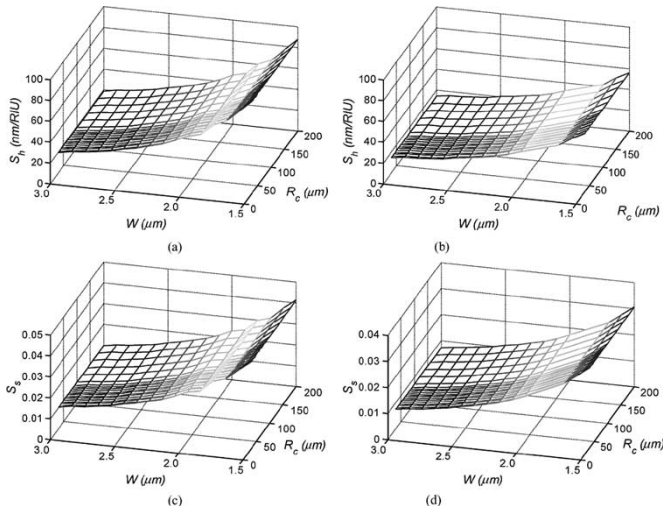

Fig. 7. Overall sensitivity plotted as a function of W and $R_{\rm c}$ for (a) TE and (b) TM fundamental modes in the case of homogeneous sensing and for (c) TE and (d) TM fundamental modes in the case of surface sensing, respectively. It is shown that a higher sensitivity requires a smaller W but has little dependence on $R_{\rm c}$.

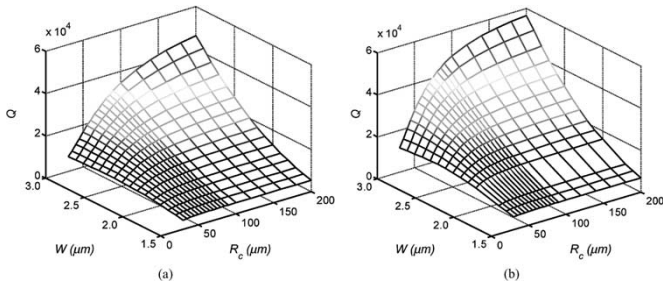

Fig. 8. Q is calculated for (a) TE and (b) TM fundamental modes.

definition, a higher Q implies a lower loss energy and a smaller FWHM. A high Q can be obtained by using a large $R_{\rm c}$ due to a linear dependence [17]. However, $R_{\rm c}$ is limited in order to have a sufficiently wide FSR. A wider waveguide width is also necessary due to better optical confinement, which can reduce the loss in a microring resonator. Since $1/P = Q \times S$ and the figures of Q show similar trends to those of $1/P$, this implies that Q has a higher domination on $1/P$ than S does. Hence, a higher Q should be the primary focus in order to achieve a lower detection limit.

B. Doubly Coupled Microring Sensor With a Fixed Gap Size

For a doubly coupled microring sensor using its drop port for detection, we fix the gap separation in the coupling area to be 250 nm. In this situation, the coupling between the bus and the ring waveguides is mainly determined by the waveguide width. To find out the optimal W and $R_{\rm c}$, we need to consider $1/P$, contrast ratio, and on-resonance dropping coefficient, as plotted in Fig. 9 for TE polarization. From these figures, a lower detection limit occurs at a larger W and $R_{\rm c}$ for both homogeneous and surface sensing, which has a similar behavior to that of singly coupled microrings. The detection limit is still dominated by Q because of its similar trend to $1/P$. However, the highest contrast ratio requires a larger W and an optimal

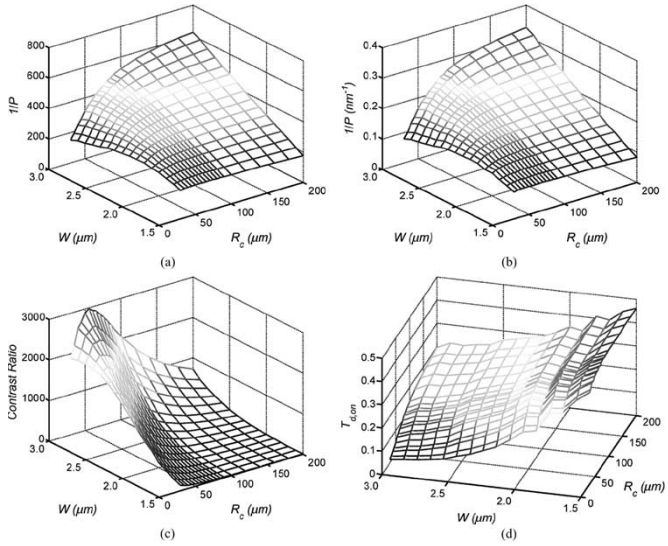

Fig. 9. Inverse of the detection factor using (a) homogeneous sensing and (b) surface sensing for the TE fundamental mode, (c) contrast ratio, and (d) on-resonance dropping coefficient for a doubly coupled microring with a fixed gap at 250 nm.

$R_{\rm c}$. To achieve a higher on-resonance dropping coefficient, a smaller W is required. Narrower waveguides provide less optical confinement but increase the overlap between the modes of the straight and the curved waveguides in the coupling region. A larger mode overlap leads to a larger cross coupling and, in turn, enhances the on-resonance dropping coefficient.

C. Doubly Coupled Microring Sensor With a Fixed On-Resonance Dropping Transmission Coefficient $t_{\rm d,on}$

From the previous example, the on-resonance dropping coefficient changes substantially with W and $R_{\rm c}$. This coefficient is very important to render a sufficiently high output signal such that an SNR can be maintained at a high value. In this example, the dropping coefficient is fixed at 0.4 to ensure a good SNR. In this situation, only $1/P$ and the contrast ratio should be considered, and the calculated results for TE polarization are plotted in Fig. 10. According to the results, a lower detection limit occurs again at a larger W and $R_{\rm c}$ for both sensing mechanisms. The Q in Fig. 10(c) shows similar trend to $1/P$ and then still dominates the influence on the detection limit. With the on-resonance dropping coefficient fixed at 0.4, the contrast ratio cannot reach as high as it does in the previous example. However, it is still sufficient to distinguish a resonance shift. In our experience, a contrast ratio of 10 is adequate for a sensor operation using microrings.

V. Discussions

For microring sensors, a lower detection limit (i.e., higher $1/P$) can be obtained by increasing both the Q (i.e., smaller resonance bandwidth) and the sensitivity. However, there is a tradeoff between a high Q and a high sensitivity. The former requires wider waveguides to provide a better optical confinement and therefore lower loss, while the latter requires narrower waveguides to achieve a stronger evanescent wave

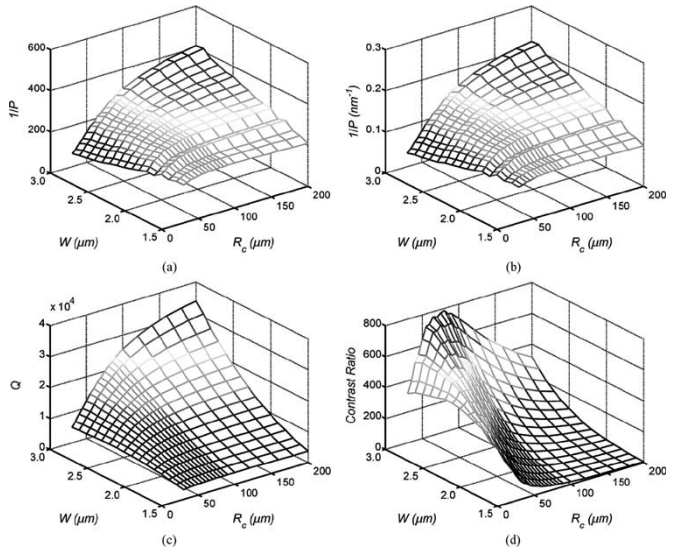

Fig. 10. Inverse of detection factor using (a) homogeneous sensing and (b) surface sensing for the TE fundamental mode, (c) Q, and (d) contrast ratio for a doubly coupled microring with a fixed on-resonance dropping coefficient at 0.4.

to interact with the analytes. Our analyses in the context of several examples conclude that the detection limit is primarily determined by the Q rather than the sensitivity parameter. Thus, it is more efficient to enhance Q for lowering the detection limit. Q can be dramatically enhanced by reducing the microring loss and/or increasing the radius of the microring.

The second important consideration is to increase the SNR. This requirement can be satisfied if the resonance has a sufficient ON–OFF contrast, which is determined by a detailed balance between the coupling of the microring to the bus waveguide and the loss in the microring. In practice, the specification of a microring sensor should be decided beforehand, such as the required detection limit, the sensitivity, the contrast ratio, and the SNR. Based on the chosen specification, an optimal range of W and R_c can be achieved by using the plots obtained in the corresponding examples.

VI. Conclusion

In this paper, we derived analytical expressions of sensitivity for microring sensors used in both homogeneous and surface sensing by measuring either the resonant-wavelength shift or the intensity variation. Based on this derivation and with the basic microring theory, the detection factor was defined and used to optimize the detection limit. To have a better sensing performance, microring sensors should have a single-mode operation and a large FSR. In addition, a low detection limit, a high sensitivity, a high contrast ratio, and a large SNR are required. The criteria of a single-mode operation and a large FSR render a parameter window for the waveguide width and the radius of microring. To further determine the optimal device structure within this window, examples of singly coupled and doubly coupled configurations were illustrated and several important parameters were calculated, including the inverse detection factor, the sensitivity, the Q, the on-resonance or nonresonance intensity, and the contrast ratio. We found that

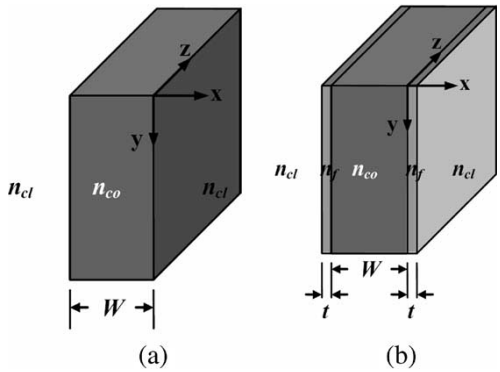

Fig. 11. Equivalent waveguide structures used in (a) homogeneous sensing and (b) surface sensing.

the detection limit is dominated by the Q of the resonance. This means that the enhancement of Q is the primary consideration to lower the detection limit. From the aforementioned examples, one can determine the specification of microring sensors and then use these figures to find out suitable ranges for W and R_c. This procedure facilitates the design and the optimization of microrings for biochemical sensing applications.

Appendix I

To calculate the sensitivity of microring sensors in homogeneous sensing, we use the field distribution in the straight waveguide to simplify that in the curved waveguide. In addition, the effective-index method is utilized to simplify a 3-D ridge waveguide into a two-dimensional (2-D) slab waveguide as shown in Fig. 11(a). With the use of the basic waveguide theory [18], the characteristic equation for TM fundamental mode can be expressed as

$$n_{\rm co}^2 \gamma_{\rm c} = n_{\rm cl}^2 k_x \tan\left(\frac{k_x W}{2}\right) \tag{11}$$

where $\gamma_{\rm c}$ and k_x are the attenuation coefficients in the cladding and the propagation constant along x-direction, respectively, and $n_{\rm co}$ and $n_{\rm cl}$ are the equivalent core and cladding indexes, respectively. From the definition of $(S_{\rm w})_{\rm h} = \partial n_{\rm eff}/\partial n_{\rm c} = \partial n_{\rm eff}/\partial n_{\rm cl}$ where $n_{\rm eff}$ and $n_{\rm c}$ are the effective index and the top-cladding index, respectively, the sensitivity can be calculated as

$$(S_{\rm w})_{\rm h,TM} = \frac{n_{\rm cl}}{n_{\rm eff}} \times \frac{1 + \frac{2\gamma_{\rm c} k_x}{n_{\rm co}^2 k_0^2} \tan\left(\frac{k_x W}{2}\right)}{1 + \frac{n_{\rm cl}^2 \gamma_{\rm c}}{n_{\rm co}^2 k_x}\left[\tan\left(\frac{k_x W}{2}\right) + \frac{k_x W}{2}\sec^2\left(\frac{k_x W}{2}\right)\right]} \tag{12}$$

where k_0 is the wave vector in vacuum. The sensitivity for the TE fundamental mode can be obtained following the same procedure. It should be noted that the TM polarization in a 2-D simplified waveguide structure has the major E field along x-direction; thus, it corresponds to the TE polarization in a real 3-D structure.

APPENDIX II

To calculate the sensitivity of microring sensors in surface sensing, the effective-index method is again used to simplify the calculation, as shown in Fig. 11(b). For this structure, TM modes have H fields in each of five regions expressed as

$$\begin{aligned} H_y &= H_{\rm cl} e^{-\gamma_c (x-t)}, \quad x \geq t \\ H_y &= H_{\rm f1} e^{-\gamma_f x} + H_{\rm f2} e^{\gamma_f x}, \qquad 0 \leq x \leq t \\ H_y &= H_{\rm co} \cos(k_x x + \phi_c), \qquad -W \leq x \leq 0 \\ H_y &= H_{\rm f1} e^{\gamma_f (x+W)} \\ &\quad + H_{\rm f2} e^{-\gamma_f (x+W)}, \qquad -W - t \leq x \leq -W \\ H_y &= H_{\rm cl} e^{\gamma_c (x+W+t)}, \qquad x \leq -W - t \end{aligned} \tag{13}$$

where $H_{\rm cl}$, $H_{\rm f1}$, $H_{\rm f2}$, $H_{\rm co}$, and ϕ_c are constants, and γ_f, t, and n_f are the attenuation coefficients in the adsorbed film, the film thickness, and refractive index of the film, respectively. To solve this waveguide structure, boundary conditions have to be satisfied, which are continuous tangential field components H_y and E_z at the interfaces. With the assumption of a thin adsorbed film, the characteristic equation can be expressed as

$$k_x W = 2 \tan^{-1} \left\{ \frac{n_{\rm co}^2 \gamma_c}{n_{\rm cl}^2 k_x} \cdot \left\{ 1 - \frac{k_0}{\gamma_c} \eta \times \left[n_{\rm eff}^2 \left(\frac{1}{n_{\rm cl}^2} + \frac{1}{n_f^2} \right) - 1 \right] \right\} \right\} + m\pi \tag{14}$$

where m is an integer. For the fundamental mode, the sensitivity can be calculated with the definition of $(S_w)_s = \partial n_{\rm eff} / \partial t$ as

$$(S_w)_{s,\rm TM}^{-1} = \frac{n_{\rm eff} (A-1)^{-2}}{n_f^2 - n_{\rm cl}^2} \times \left\{ -\frac{2A}{k_0^2 n_{\rm eff}^2} \cdot \left[\gamma_c - \frac{n_{\rm cl}^2}{n_{\rm co}^2} k_x B \right] + (A-1) \times \left[\frac{1}{\gamma_c} + \frac{W n_{\rm cl}^2}{2 n_{\rm co}^2} (1 + B^2) + \frac{n_{\rm cl}^2}{n_{\rm co}^2 k_x} B \right] \right\} \tag{15}$$

where

$$A \equiv n_{\rm eff}^2 \left(\frac{1}{n_{\rm cl}^2} + \frac{1}{n_f^2} \right) \tag{16}$$

and

$$B \equiv \tan \left(\frac{k_x W}{2} \right). \tag{17}$$

REFERENCES

[1] T. Okamoto, M. Yamamoto, and I. Yamaguchi, "Optical waveguide absorption sensor using a single coupling prism," *J. Opt. Soc. Amer. A, Opt. Image Sci.*, vol. 17, no. 10, pp. 1880–1886, Oct. 2000.

[2] B. J. Luff, R. D. Harris, J. S. Wilkinson, R. Wilson, and D. J. Schiffrin, "Integrated-optical directional coupler biosensor," *Opt. Lett.*, vol. 21, no. 8, pp. 618–620, Apr. 1996.

[3] Z. Qi, N. Matsuda, K. Itoh, M. Murabayashi, and C. R. Lavers, "A design for improving the sensitivity of a Mach–Zehnder interferometer to chemical and biological measurands," *Sens. Actuators B, Chem.*, vol. 81, no. 2, pp. 254–258, Jan. 2002.

[4] R. Hornath, H. C. Pedersen, N. Skivesen, D. Selmeczi, and N. B. Larsen, "Optical waveguide sensor for on-line monitoring of bacteria," *Opt. Lett.*, vol. 28, no. 14, pp. 1233–1235, Jul. 2003.

[5] ——, "Monitoring of living cell attachment and spreading using reverse symmetry waveguide sensing," *Appl. Phys. Lett.*, vol. 86, no. 7, p. 071101, Feb. 2005.

[6] E. Krioukov, D. J. W. Klunder, A. Driessen, J. Greve, and C. Otto, "Integrated optical microcavities for enhanced evanescent-wave spectroscopy," *Opt. Lett.*, vol. 27, no. 17, pp. 1504–1506, Sep. 2002.

[7] ——, "Sensor based on an integrated optical microcavity," *Opt. Lett.*, vol. 27, no. 17, pp. 512–514, Apr. 2002.

[8] F. Vollmer, D. Braun, A. Libchaber, M. Khoshsima, I. Teraoka, and S. Arnold, "Protein detection by optical shift of a resonant microcavity," *Appl. Phys. Lett.*, vol. 80, no. 21, pp. 4057–4059, May 2002.

[9] S. Arnold, M. Khoshsima, I. Teraoka, S. Holler, and F. Vollmer, "Shift of whispering-gallery modes in microspheres by protein adsorption," *Opt. Lett.*, vol. 28, no. 4, pp. 272–274, Feb. 2003.

[10] C.-Y. Chao and L. J. Guo, "Biochemical sensors based on polymer microrings with sharp asymmetrical resonance," *Appl. Phys. Lett.*, vol. 83, no. 8, pp. 1527–1529, Aug. 2003.

[11] S. Blair and Y. Chen, "Resonant-enhanced evanescent-wave fluorescence biosensing with cylindrical optical cavities," *Appl. Opt.*, vol. 40, no. 4, pp. 570–582, Nov. 2001.

[12] R. W. Boyd and J. E. Heebner, "Sensitive disk resonator photonic biosensor," *Appl. Opt.*, vol. 40, no. 31, pp. 5742–5747, Nov. 2001.

[13] K. Okamoto, *Fundamentals of Optical Waveguides*. San Diego, CA: Academic, 2000, ch. 2.

[14] C.-Y. Chao, W. Fung, and L. J. Guo, "High Q-factor polymer microring resonators used in the biochemically sensing applications," *IEEE J. Sel. Topics Quantum Electron.* submitted for publication.

[15] C.-Y. Chao and L. J. Guo, "Polymer microring resonators fabricated by nanoimprint technique," *J. Vac. Sci. Technol. B, Microelectron. Process. Phenom.*, vol. 20, no. 6, pp. 2862–2866, Nov./Dec. 2002.

[16] ——, "Reduction of surface scattering loss in polymer microrings using thermal-reflow technique," *IEEE Photon. Technol. Lett.*, vol. 16, no. 6, pp. 1498–1500, Jun. 2004.

[17] B. E. Little, S. T. Chu, H. A. Haus, J. Foresi, and J.-P. Laine, "Microring resonator channel dropping filters," *J. Lightw. Technol.*, vol. 15, no. 6, pp. 998–1005, Jun. 1997.

[18] H. Nishihara, M. Haruna, and T. Suhara, *Optical Integrated Circuits*. New York: McGraw-Hill, 1989, ch. 2.

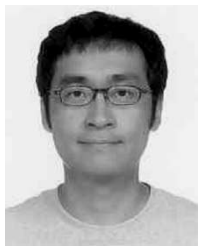

Chung-Yen Chao was born in Taipei, Taiwan, R.O.C., in 1973. He received the B.S. degree in electrical engineering and the M.S. degree in electro-optical engineering from the National Taiwan University, Taipei, in 1995 and 1997, respectively, and the Ph.D. degree from the Solid State Electronics Laboratory, University of Michigan, Ann Arbor, in 2004.

His research interests include nanofabrication technology and the design and fabrication of integrated optical devices in the applications of telecommunication, biochemical sensing, and medical diagnoses.

L. Jay Guo (M'98) received the Ph.D. degree from the University of Minnesota, Minneapolis, in 1997.

From 1997 to 1999, he was a Research Associate at Princeton University, Princeton, NJ. In 1999, he joined the Department of Electrical Engineering and Computer Science, University of Michigan, Ann Arbor, as an Assistant Professor. His current research areas include organic electronics, nanoimprinting, nanophotonics, and nanofabrication technologies with applications in polymer photonic devices and biotechnologies.